Measurements of W and Z boson production in ATLAS

Zhibo Wu[1,2⋆], on behalf of the ATLAS Collaboration

1 IRFU CEA Paris-Saclay, 91190 Gif Sur Yvette, France
2 University of Science and Technology of China, Hefei, China

⋆ zhibo.wu@cern.ch

*Proceedings for the XXVIII International Workshop
on Deep-Inelastic Scattering and Related Subjects,
Stony Brook University, New York, USA, 12-16 April 2021*

Abstract

Precision measurements of the production cross-sections of W and Z boson at LHC provide important tests of perturbative QCD and information about the parton distribution functions for quarks within the proton. We present measurements of cross sections for inclusive W^+, W^- and Z boson production using data collected by the ATLAS experiment at a center-of-mass energy of $\sqrt{s}$=2.76 TeV. Measurement of the transverse momentum distribution of Z boson at $\sqrt{s}$=13 TeV is also presented. The measurements are corrected for detector effects and compared with state-of-the-art theoretical calculations.

1 Introduction

The measurements of W and Z production are of high importance in the Standard Model Electroweak sector. The relevant measurements not only allow to probe important parameters such as W mass and weak mixing angle, but also allow to check the consistency of the Standard Model, for instance, lepton universality. At lowest order in QCD, W and Z bosons are produced in proton-proton collisions through quark anti-quark annihilation: a pair of quark and anti-quark of the same flavor for Z production; one quark and one anti-quark of another flavor for W production. Higher-order QCD processes lead to non-zero p_{T} distributions of vector bosons. Given that the production of W/Z depends on low p_{T} non-perturbative QCD processes, the measurements of W and Z production therefore allow to probe both perturbative and and non-perturbative QCD predictions. In addition, the measured production cross-sections are supposed to place constraints on PDF as well.

Section 2 below will give a brief description of the W and Z event topologies at the Large Hadron Collider (LHC). Then the two ATLAS [1] measurements will be reviewed in the following sections: Section 3 focuses on the measurement of W and Z production at $\sqrt{s}$=2.76 TeV [2]. The measurement of Z-boson transverse momentum at $\sqrt{s}$=13 TeV [3] is introduced in section 4. Conclusions of these two measurements are summarized in section 5.

2 Event topologies

Only leptonic decays of W and Z bosons are selected for precision measurements in proton-proton collisions, where the decay leptons flavour is restricted to only electron and muon.

The leptonic decay of W-boson yields one charged lepton and one neutrino in the final state. Since the transverse momentum of the neutrino cannot be detected, it is inferred from the vector of the missing transverse momentum $\overrightarrow{E}_\mathrm{T}^{\,\mathrm{miss}}$, which is the negative vector sum of the lepton transverse momentum $\overrightarrow{p}_\mathrm{T}^{\,l}$ and of the hadronic recoil $\overrightarrow{u}_\mathrm{T}$:

$$\overrightarrow{E}_\mathrm{T}^{\,\mathrm{miss}} = -(\overrightarrow{p}_\mathrm{T}^{\,l} + \overrightarrow{u}_\mathrm{T}). \tag{1}$$

The hadronic recoil $\overrightarrow{u}_\mathrm{T}$ is defined as the vector sum of all topo-clusters in the calorimeters, excluding those from the signal charged lepton. The W transverse mass, m_T^W, is an important observable that is derived from the lepton transverse momentum and from the missing transverse momentum:

$$m_\mathrm{T}^\mathrm{W} = \sqrt{2p_\mathrm{T}^l E_\mathrm{T}^\mathrm{miss}(1 - \cos(\phi_l - \phi_{E_\mathrm{T}^\mathrm{miss}}))}. \tag{2}$$

Here $\phi_l - \phi_{E_\mathrm{T}^\mathrm{miss}}$ is the azimuthal angle between the charged lepton and the missing transverse momentum.

In Z-boson decays, both leptons are detected, which gives an invariant mass of the lepton pair peaked around the Z mass.

3 Measurement of W/Z production cross-sections at 2.76 TeV with the ATLAS detector

3.1 Data and simulation samples

The data of this measurement were collected in February 2013 at $\sqrt{s}$=2.76 TeV with an average pile-up of 0.3. The typical value of instantaneous luminosity in this data-taking period, $1 \times 10^{32}\,\mathrm{cm}^{-2}\,\mathrm{s}^{-1}$, is lower than in the 7, 8 and 13 TeV usual conditions, yielding to a dataset of $4\,\mathrm{pb}^{-1}$. In the MC simulation, the signal samples are generated by POWHEG-BOX v1 r1556 [4–7], with a parton shower performed by PYTHIA8.17 [8]. For the background processes, the $t\bar{t}$ samples are simulated by POWHEG-BOX v1 r2330 [9] and di-boson (WW, ZZ, WZ) production is produced by HERWIG6.5 [10]. The sample cross-sections are normalized to the NNLO QCD predictions.

3.2 Event selection

In this measurement, the electrons are reconstructed by clusters of energy in the EM calorimeter and are matched to tracks in the Inner-Detector (ID). The signal electrons are required to have their transverse momentum higher than 20 GeV and their pseudorapidity $|\eta|$ lower than 2.4, excluding the transition region (1.37<$|\eta|$<1.52) between the barrel and the endcap calorimeters. Muons are reconstructed by combining the tracks in the Muon Spectrometer (MS) and those in the ID. The signal muons are required to have p_T larger than 20 GeV and $|\eta|$ below 2.4. The W event selection further requires $E_\mathrm{T}^\mathrm{miss}$ to be higher than 25 GeV and m_T to be higher than 40 GeV. In the Z event selection, the desired invariant mass of the lepton pair is required to be between 66 GeV and 116 GeV. Table 1 presents the summary of the number of observed candidates and estimated background in each channel. The electroweak

background contribution and the background coming from top quark related processes are estimated by the simulation, while the multijet background in W channels is derived from data. The methodology of the multijet estimation is further illustrated in the next subsection.

Table 1: Number of observed candidates and total background contributions for both the W and Z decay channels (Numbers are taken from [2]). The background fractions in the Z channels are much lower than those in the W channels.

Measurement channel	Observed candidates	Total background	Background fraction
$W^+ \rightarrow e^+ \nu$	3914	138 ± 12	3.5%
$W^- \rightarrow e^- \nu$	2209	104 ± 12	4.7%
$W^+ \rightarrow \mu^+ \nu$	4365	155 ± 7	3.5%
$W^- \rightarrow \mu^- \nu$	2460	110 ± 5	4.5%
$Z \rightarrow e^+ e^-$	430	1.3 ± 0.0	0.3%
$Z \rightarrow \mu^+ \mu^-$	646	1.6 ± 0.1	0.2%

3.3   Multijet background estimation

Due to the fact that the contribution of multijet background is negligible in the Z decay channels, this estimation is only implemented in the W channels. The shape (template) of the multijet background in the electron channel is derived using the E_T^miss spectra in a control region where the electron identification is inverted and where the E_T^miss cut has been removed. Therefore, this multijet-enriched control region is statistically independent of the signal region. The template in muon channels is derived using the m_T spectra in a control region where the muon isolation is inverted and the m_T cut is removed. The multijet shape is extracted in the control regions by subtracting the simulated contributions of signal and other backgrounds.

The normalization of multijet in the signal region is computed by a χ^2 minimization of the multijet templates to the sum of the signal, multijet and other background components. The overall number of multijet background is estimated from the fit to the total W-boson samples.

3.4   Correction for detector effects

The fiducial production cross-section is calculated by dividing the number of signal events by the integrated luminosity, corrected for the detection efficiency. The value of the detection efficiency C_W is about 0.67 for $W \rightarrow e\nu$ and 0.75 for $W \rightarrow \mu\nu$. Meanwhile C_Z is 0.55 for $Z \rightarrow e^+ e^-$ and 0.79 for $Z \rightarrow \mu^+ \mu^-$. The total production cross-section in each channel is extrapolated from the fiducial cross-section by applying an acceptance correction. The acceptance corrections are determined from the signal MC samples, and turn out to be around 0.6.

Among all the systematic uncertainties in the efficiency factor, the muon trigger (1.1% for $W \rightarrow \mu\nu$) as well as the electron reconstruction and identification (2.3% for $W \rightarrow e\nu$ and 4.6% for $Z \rightarrow ee$) uncertainties are the dominant components. The η-independent muon trigger efficiency is determined by the tag-and-probe method [11] in the 2.76 TeV dataset, while the electron reconstruction and identification efficiencies are extrapolated from the tag-and-probe estimations in 8 TeV data to the 2.76 TeV dataset [12, 13].

For the acceptance factor, the uncertainty due to the choice of the PDF set ranges from 1% to 1.4% depending on the channel. The choice of event generator and parton shower models adds an additional uncertainty of 0.9% on the acceptance correction.

3.5 Results

Figure 1 shows the fiducial cross-sections of (a) W^+, (b) W^-, (c) $W^\pm$ combined and (d) Z, where generally good agreement between the measurement and theory predictions is observed. The results obtained from the electron and muon final states are also consistent with each other. The total production cross-sections are extrapolated to the full phase space thanks to the acceptance factor, as shown in Figure 2.
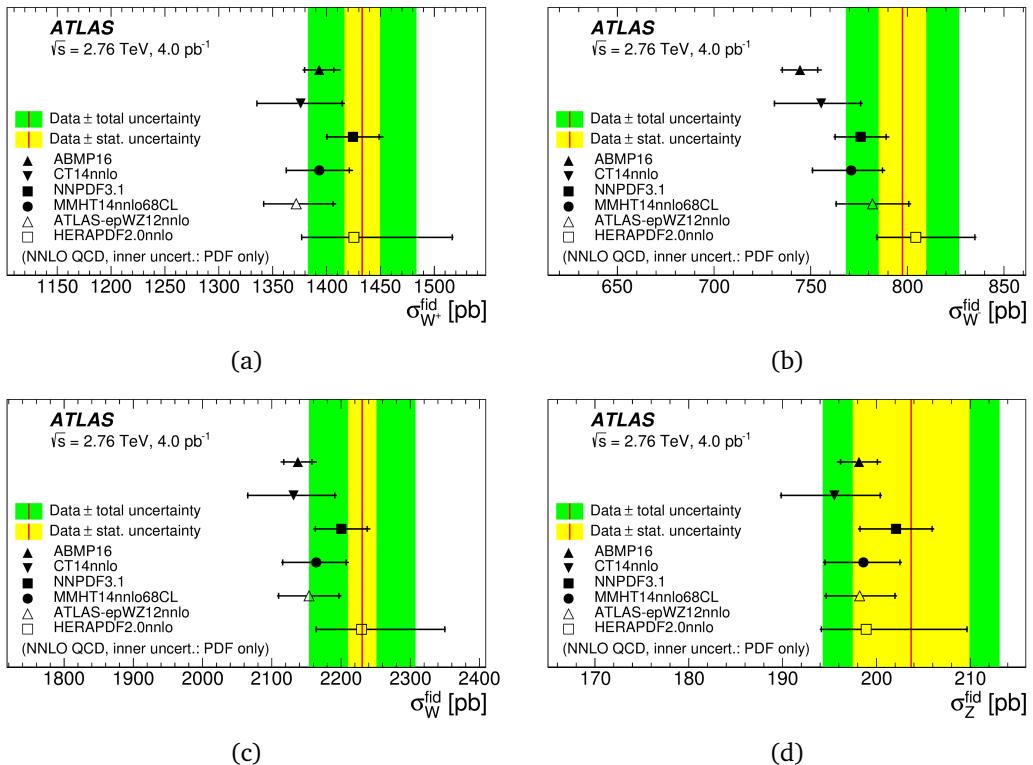
Figure 1: NNLO predictions for the fiducial cross-section compared with the measured cross-section of (a) W^+, (b) W^-, (c) $W^\pm$ combined and (d) Z. Plots are taken from [2].

The cross-sections are usually presented in the form of ratios in order to benefit from the cancellation of systematics. The test of lepton universality is based on the ratio of fiducial production cross-sections of electron channel over muon channel for W and Z decay events:

$$R_{W^+} = \sigma^{\text{fid}}_{W \to e^+ \nu} / \sigma^{\text{fid}}_{W \to \mu^+ \nu} = 0.985 \pm 0.023 \,(\text{stat.}) \pm 0.028 \,(\text{syst.})$$

$$R_{W^-} = \sigma^{\text{fid}}_{W \to e^- \nu} / \sigma^{\text{fid}}_{W \to \mu^- \nu} = 0.988 \pm 0.030 \,(\text{stat.}) \pm 0.028 \,(\text{syst.})$$

$$R_W = \sigma^{\text{fid}}_{W \to e \nu} / \sigma^{\text{fid}}_{W \to \mu \nu} = 0.986 \pm 0.018 \,(\text{stat.}) \pm 0.028 \,(\text{syst.})$$

$$R_Z = \sigma^{\text{fid}}_{Z \to e^+ e^-} / \sigma^{\text{fid}}_{Z \to \mu^+ \mu^-} = 0.96 \pm 0.06 \,(\text{stat.}) \pm 0.05 \,(\text{syst.}).$$

The above results stay within one standard deviation of the Standard Model prediction and previous measurement performed by ATLAS [14].

(a)   (b)
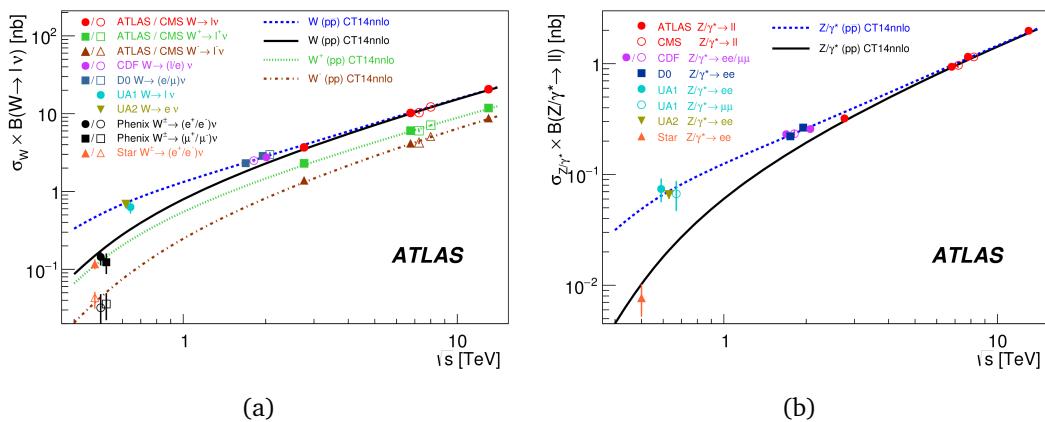
Figure 2: The measurements of (a) $\sigma_W \times B(W \to l\,\nu)$ and (b) $\sigma_{Z/\gamma^*} \times B(Z/\gamma^* \to ll)$ for both proton-proton and proton-antiproton collisions at various center-of-mass energies. The data points are compared with theoretical calculations at NNLO in QCD. Plots are taken from [2].

Another two important ratios are the ratio of the combined W cross-section over the Z cross-section and the ratio of W^+ over W^-:

$$R_{W/Z} = 10.95 \pm 0.35\,(\text{stat.}) \pm 0.10\,(\text{syst.})$$
$$R_{W^+/W_-} = 1.797 \pm 0.034\,(\text{stat.}) \pm 0.009\,(\text{syst.}).$$

These two ratios put constraints on the strange quark distribution within the proton and on the valence quarks distributions, respectively. Although the results of this measurement are dominated by statistical uncertainties, in other measurements at higher energies such as [14, 15], the statistical uncertainty is much smaller thanks to the larger data set.

The charge asymmetry in W-boson production is commonly expressed by the ratio of W^+ cross-section over W^- cross-section, which also benefits from the cancellation of systematic uncertainties:

$$A_l = \frac{\sigma_{W^+}^{\text{fid}} - \sigma_{W^-}^{\text{fid}}}{\sigma_{W^+}^{\text{fid}} + \sigma_{W^-}^{\text{fid}}} = 0.285 \pm 0.009\,(\text{stat.}) \pm 0.002\,(\text{syst.}).$$

4 Measurement of Z-boson transverse momentum at 13 TeV with the ATLAS detector

4.1 Definitions of observables

The distributions of two observables are measured in this work, specifically the transverse momentum of Drell-Yan lepton pair, p_T^{ll}, as well as the angular variable Φ_η^*. A precise measurement of p_T^{ll} is important for both Beyond Standard Model searches, to evaluate the Standard Model background at high p_T, and Standard Model precision measurement (low p_T region). An alternative observable:

$$\Phi_\eta^* = \tan\left(\frac{\pi - \Delta\Phi}{2}\right) \times \sin(\theta_\eta^*),$$

where $\Delta\Phi$ is the azimuthal angle between the two leptons and where $\cos(\theta_\eta^*) = \tanh[(\eta^- - \eta^+)/2]$ relies on the pseudorapidities of negatively and positively charged

leptons, is introduced since it depends exclusively on the directions of the two leptons. The measurement of this observable has the advantage, compared to p_T^{ll}, that in the low p_T^{ll} region it doesn't suffer from a relatively worse lepton momentum resolution.

4.2 Data and simulation samples

The analysis uses the data collected in 2015 and 2016 at $\sqrt{s} =$13 TeV corresponding to an integrated luminosity of 36 pb^{-1}. The MC signals are simulated by the POWHEG-BOX V1 MC event generator at NLO in α_S interfaced to PYTHIA8.186 [16]. POWHEG+PYTHIA8 is also used to simulate most of the background processes [17].

4.3 Event selection

Electron candidates are reconstructed by clusters of energy in the EM calorimeter matched to ID tracks. The fiducial cuts for the electrons are the following: p_T higher than 27 GeV, $|\eta|$ lower than 2.47 skipping the transition region of the calorimeter. Muon candidates are reconstructed by combining MS and ID tracks. The muon p_T has to be larger than 27 GeV. The $|\eta|$ range is required to be within 2.5. Furthermore, the selection of Z event requires two same-flavor-opposite-sign leptons with an invariant mass between 66 GeV and 116 GeV.

The number of events and estimated background components are listed in Table 2. The fraction of background is less than 1% in both the $Z \rightarrow ee$ and $Z \rightarrow \mu\mu$ channels. Di-boson and top-quark related processes are estimated to be the dominant background sources according to simulation. The multijet processes are estimated by data-driven techniques for both decay channels.

Table 2: Numbers of observed candidates and total background contributions for the $Z \rightarrow ee$ and $Z \rightarrow \mu\mu$ decay channels (from [3]).

Measurement channel	Observed candidates	Total background	Background fraction
$Z/\gamma^* \rightarrow e^+e^-$	13 649 239	89 400 ± 5600	0.7%
$Z/\gamma^* \rightarrow \mu^+\mu^-$	18 162 641	100 500 ± 3300	0.6%

4.4 Correction for detector effects

The fiducial cross-sections are the number of signal events divided by luminosity and corrected for detection efficiency. Final differential distributions are extracted, using Bayesian unfolding to correct for detector effects. The response matrix and the correction for reconstruction efficiency are derived from signal MC samples.

While the theory and modelling uncertainties are negligible, the systematic uncertainties in the detection efficiency corrections are dominated by lepton identification and reconstruction efficiencies, which are 0.5% for the $Z \rightarrow ee$ channel and 1% for the $Z \rightarrow \mu\mu$ channel.

4.5 Results

The measured fiducial cross-sections in individual channels are combined at Born level in Table 3. The prediction [18] made at NNLO in α_S using the CT14 PDF set is comparable to the combined cross-section within uncertainties. The Born-level combined measurements of normalized distributions are compared to different predictions in Figure 3, among which the

Table 3: Measured integrated fiducial cross section in electron and muon decay channels at Born level as well as the combination (from [3]). The prediction at NNLO in α_S uses the CT14 PDF set.

Channel	Measured cross-section×$B(Z/\gamma^* \to ll)$ (value ± stat. ± syst. ± lumi.)	Predicted cross-section×$B(Z/\gamma^* \to ll)$ (value ± PDF ± α_S ± scale ± intrinsic)
$Z/\gamma^* \to ee$	$738.3 \pm 0.2 \pm 7.7 \pm 15.5$ pb	
$Z/\gamma^* \to \mu\mu$	$731.7 \pm 0.2 \pm 11.3 \pm 15.3$ pb	
$Z/\gamma^* \to ll$	$736.2 \pm 0.2 \pm 6.4 \pm 15.5$ pb	$703^{+19+6+4+5}_{-24-8-6-5}$ pb

RADISH program [19, 20] combines a fixed NNLO order prediction of the Z+jet cross section with resummation of the $\log(m_{ll}/p_T^{ll})$ terms at next-to-next-to-next-to-leading-logarithm (N^{3}LL) accuracy. Except for larger uncertainties in the low p_T^{ll} and low Φ_η^* region, the RADISH prediction agrees with the data over the full spectra with uncertainties typically from 1 to 3 percent.
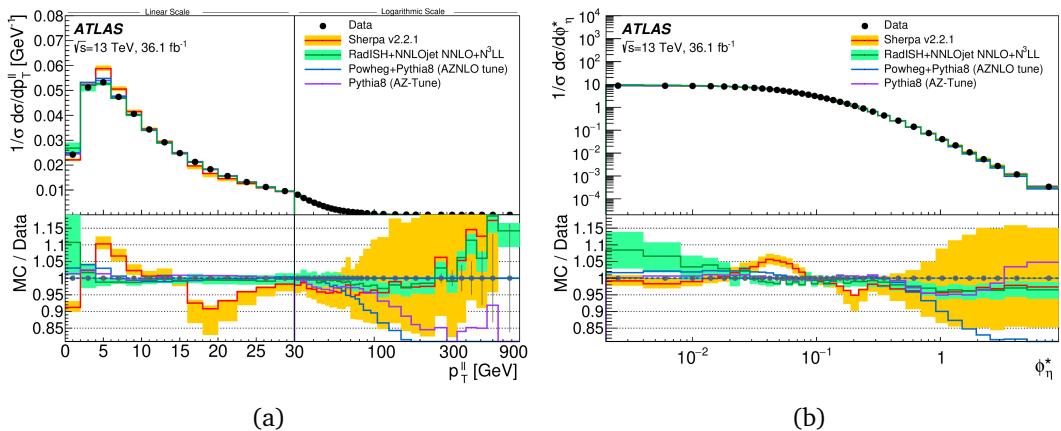
Figure 3: Comparison of normalized (a) p_T^{ll} and (b) Φ_η^* distributions predicted by various computations. The uncertainties of Sherpa and Radish predictions are presented by error bands. Plots are taken from [3].

5 Conclusion

This article reviewed the state-of-the-art ATLAS measurement of W and Z production cross-sections at 2.76 TeV as well as the measurement of transverse momentum distribution of Drell-Yan lepton pair at 13 TeV, using proton-proton collision data at LHC.

At 2.76 TeV, the production cross-sections for W and Z bosons are measured in fiducial regions and then extrapolated to the full phase space. Measured ratios and asymmetries composed of fiducial cross-sections are also reported, all in agreement with NNLO QCD calculations. In the measurement of p_T^{ll} and Φ_η^* of Drell-Yan lepton pairs at 13 TeV, the data agrees with QCD prediction based on resummation approaches within uncertainties.

References

[1] ATLAS Collaboration, *The ATLAS Experiment at the CERN Large Hadron Collider*, J. Inst. **3**, S08003 (2008), doi:10.1088/1748-0221/3/08/s08003.

[2] ATLAS COllaboration, *Measurement of $W^{\pm}$-boson and Z-boson production cross-sections in pp collisions at $\sqrt{s} = 2.76\,TeV$ with the ATLAS detector*, Eur. Phys. J. C **79**, 901 (2019), doi:10.1140/epjc/s10052-019-7399-7.

[3] ATLAS Collaboration, *Measurement of the transverse momentum distribution of Drell–Yan lepton pairs in proton–proton collisions at $\sqrt{s} = 13\,TeV$ with the ATLAS detector*, Eur. Phys. J. C **80**, 616 (2020), doi:10.1140/epjc/s10052-020-8001-z.

[4] P. Nason, *A New Method for Combining NLO QCD with Shower Monte Carlo Algorithms*, J. High Energy Phys. **11**, 040 (2004), doi:10.1088/1126-6708/2004/11/040.

[5] S. Frixione, P. Nason and C. Oleari, *Matching NLO QCD computations with parton shower simulations: the POWHEG method*, J. High Energy Phys. **11**, 070 (2007), doi:10.1088/1126-6708/2007/11/070.

[6] S. Alioli, P. Nason, C. Oleari and E. Re, *A general framework for implementing NLO calculations in shower Monte Carlo programs: the POWHEG BOX*, J. High Energy Phys. **06**, 043 (2010), doi:10.1007/JHEP06(2010)043.

[7] S. Alioli, P. Nason, C. Oleari and E. Re, *NLO vector-boson production matched with shower in POWHEG*, J. High Energy Phys. **07**, 060 (2008), doi:10.1088/1126-6708/2008/07/060.

[8] T. Sjöstrand, S. Mrenna and P. Skands, *A brief introduction to PYTHIA 8.1*, Comput. Phys. Commun. **178**, 852 (2008), doi:10.1016/j.cpc.2008.01.036.

[9] S. Frixione, G. Ridolfi and P. Nason, *A positive-weight next-to-leading-order Monte Carlo for heavy flavour hadroproduction*, J. High Energy Phys. **09**, 126 (2007), doi:10.1088/1126-6708/2007/09/126.

[10] G. Corcella, I. Knowles, G. Marchesini, S. Moretti, K. Odagiri, P. Richardson, M. Seymour and B. Webber, *HERWIG 6.5 Release Note*, arXiv:hep-ph/0210213v2.

[11] ATLAS Collaboration, *Measurement of the muon reconstruction performance of the ATLAS detector using 2011 and 2012 LHC proton–proton collision data*, Eur. Phys. J. C **74**, 3130 (2014), doi:10.1140/epjc/s10052-014-3130-x.

[12] ATLAS Collaboration, *Electron efficiency measurements with the ATLAS detector using 2012 LHC proton–proton collision data*, Eur. Phys. J. C **77**, 195 (2017), doi:10.1140/epjc/s10052-017-4756-2.

[13] ATLAS Collaboration, *easurement of differential cross sections and W^{+}/W^{-} cross-section ratios for W boson production in association with jets at $\sqrt{s} = 8\,TeV$ with the ATLAS detector*, J. High Energy Phys. **05**, 077 (2018), doi:10.1007/JHEP05(2018)077.

[14] G. Aad et al., *Measurement of $W^{\pm}$ and Z-boson production cross sections in pp collisions at $\sqrt{s} = 13\,TeV$ with the ATLAS detector*, Phys. Lett. B **759**, 601 (2016), doi:10.1016/j.physletb.2016.06.023.

[15] ATLAS Collaboration, *Precision measurement and interpretation of inclusive W^+, W^- and Z/γ^* production cross sections with the ATLAS detector*, Eur. Phys. J. C **77**, 367 (2017), doi:10.1140/epjc/s10052-017-4911-9.

[16] T. Sjöstrand et al., *An introduction to PYTHIA 8.2*, Comput. Phys. Commun. **191**, 159 (2015), doi:10.1016/j.cpc.2015.01.024.

[17] P. Nason and G. Zanderighi, *W^+W^-, WZ and ZZ production in the POWHEG-BOX-V2*, Eur. Phys. J. C **74**, 2702 (2014), doi:10.1140/epjc/s10052-013-2702-5.

[18] ATLAS Collaboration, *Measurements of top-quark pair to Z-boson cross-section ratios at $\sqrt{s} = 13, 8, 7$ TeV with the ATLAS detector*, J. High Energy Phys. **02**, 117 (2017), doi:10.1007/JHEP02(2017)117.

[19] W. Bizoń, A. Gehrmann-De Ridder, T. Gehrmann, N. Glover, A. Huss, P. Francesco Monni, E. Re, L. Rottoli and D. M. Walker, *The transverse momentum spectrum of weak gauge bosons at N^3LL+NNLO*, Eur. Phys. J. C **79**, 868 (2019), doi:10.1140/epjc/s10052-019-7324-0.

[20] W. Bizoń et al., *Fiducial distributions in Higgs and Drell-Yan production at N^3LL+NNLO*, J. High Energy Phys. **12**, 132 (2018), doi:10.1007/JHEP12(2018)132.